

Vision Graph Non-Contrastive Learning for Audio Deepfake Detection with Limited Labels

Falih Gozi Febrinanto^{*†}, Kristen Moore[†], Chandra Thapa[†], Jiangang Ma^{*}, Vidya Saikrishna^{*}, Feng Xia^{†(✉)}

^{*}Institute of Innovation, Science and Sustainability, Federation University Australia, Ballarat, Australia

[†]CSIRO’s Data61, Australia

[‡]School of Computing Technologies, RMIT University, Melbourne, Australia

Emails: {f.febrinanto, j.ma, v.saikrishna}@federation.edu.au, {kristen.moore, chandra.thapa}@data61.csiro.au, f.xia@ieee.org

Abstract—Recent advancements in audio deepfake detection have leveraged graph neural networks (GNNs) to model frequency and temporal interdependencies in audio data, effectively identifying deepfake artifacts. However, the reliance of GNN-based methods on substantial labeled data for graph construction and robust performance limits their applicability in scenarios with limited labeled data. Although vast amounts of audio data exist, the process of labeling samples as genuine or fake remains labor-intensive and costly. To address this challenge, we propose **SIGNL**¹ (Spatio-temporal v**ision** Graph Non-contrastive Learning), a novel framework that maintains high GNN performance in low-label settings. SIGNL constructs spatio-temporal graphs by representing patches from the audio’s visual spectrogram as nodes. These graph structures are modeled using vision graph convolutional (GC) encoders pre-trained through graph non-contrastive learning, a label-free that maximizes the similarity between positive pairs. The pre-trained encoders are then fine-tuned for audio deepfake detection, reducing reliance on labeled data. Experiments demonstrate that SIGNL outperforms state-of-the-art baselines across multiple audio deepfake detection datasets, achieving the lowest Equal Error Rate (EER) with as little as 5% labeled data. Additionally, SIGNL exhibits strong cross-domain generalization, achieving the lowest EER in evaluations involving diverse attack types and languages in the In-The-Wild dataset.

Index Terms—Audio deepfake detection, graph neural networks, limited label learning, non-contrastive learning, graph-based augmentations.

I. INTRODUCTION

Recent advancements in audio deepfake technologies, such as text-to-speech (TTS) algorithms [1], [2] and voice conversion techniques [3], [4], have significantly enhanced the quality of synthetic speech. These technologies have enabled diverse applications, including audiobook services, voice assistants, and personalized content creation [5]. However the rise of synthetic audio has also introduced critical cybersecurity risks, such as spoofing attacks against automatic speaker verification (ASV) systems and scams targeting individuals [6], [7]. These threats necessitate the development of robust methods for detecting audio deepfakes to mitigate malicious exploitation.

Graph Neural Networks (GNNs) for Audio Deepfake Detection. Among deep learning techniques used for audio deepfake detection—such as convolutional neural networks (CNN) [8], [9], deep residual networks (ResNet) [10], [11],

and transformers [12]—GNNs have emerged as a highly effective approach [13], [14]. By modeling frequency sub-bands and temporal segments as graph structures, GNNs can capture irregular and complex relationships, enabling the detection of subtle deepfake artifacts that may span multiple frequency sub-bands and temporal segments [13]–[15]. Early implementations relied on visual representations of audio data (eg. spectrograms) segmented into patches, which formed the basis of graph construction [13], [16], [17]. Recent advancements have introduced more sophisticated techniques, such as integrating heterogeneous spectral and temporal sub-graphs [14] and hybrid frameworks combining learnable visual representations with GNN classifiers [18], [19].

Challenges with GNNs. Despite their effectiveness, GNN-based approaches for audio deepfake detection face critical challenges due to their heavy reliance on labeled data for graph construction and training [13], [14]. However, *labeled data is often scarce* [7], [20], resulting in overfitting and poor generalization, particularly when the model encounters new attack types or datasets [6]. Furthermore, the process of manually labeling audio data is both costly and time-intensive [21], resulting in reduced performance of supervised GNN-based models in real-world scenarios due to insufficient labeled training data [22]. Although data augmentation techniques, such as adding background noise or codec transformations [23], [24], aim to enhance diversity, these modifications often fail to introduce meaningful variations in graph structures [25].

Opportunities in non-contrastive learning. Self-supervised learning (SSL) offers a promising way to leverage large amounts of unlabeled data, reducing reliance on costly human-annotations [22]. Among SSL techniques, non-contrastive learning has shown particular promise in the computer vision domain [26], [27]. Unlike contrastive learning, non-contrastive methods do not rely on negative samples for pre-training, avoiding the risk of false negatives that can push similar samples apart [28]. Non-contrastive methods offer several additional advantages: by generating positive pairs through augmentations, they enhance data diversity, addressing the challenges associated with limited labeled datasets. Furthermore, non-contrastive learning enables a self-supervised pre-training process, allowing models to learn robust representations that can be fine-tuned with minimal labeled data, significantly reducing dependence

¹We will make our implementation code publicly available upon acceptance of this paper.

on annotations.

These methods have achieved competitive performance across various edge, node, and graph-level tasks [29], [30], but require domain-specific adaptations to construct meaningful graph structures, embeddings and augmentations for audio data [29], [31].

Our Contribution. In this work, we present SIGNAL (Spatio-temporal vision Graph Non-contrastive Learning), a novel framework designed to address the challenges posed by limited labeled data in audio deepfake detection. In contrast to existing GNN-based approaches that predominantly focus on building robust classifiers [13], [19], SIGNAL prioritises improving graph embedding quality, thereby enhancing performance in label-scarce scenarios.

SIGNAL transforms audio data into spatio-temporal graphs by segmenting visual representations (e.g., spectrograms) into spatial and temporal patches, which are represented as nodes with feature vectors. These nodes are used to form separate spatial and temporal graph structures that effectively capture intricate inter dependencies within the data. The framework employs vision graph convolution (GC) encoders pre-trained using non-contrastive learning, a strategy that maximises the similarity between augmented positive graph pairs. This eliminates the reliance on negative samples while achieving performance comparable to traditional contrastive methods for graph-level tasks [29]. By learning rich representations from diverse augmented graph views during pretraining, SIGNAL equips the encoders to be fine-tuned effectively for audio deepfake detection, even in scenarios with limited labeled data. The key contributions of this work are as follows:

- We introduce the SIGNAL framework, a novel spatio-temporal vision graph non-contrastive learning method that effectively models inter-frequency and temporal dependencies, enabling robust audio deepfake detection, even in label-scarce scenarios.
- We propose the *utilization of positive pairs of spatio-temporal graph data*, constructed from visual representations of audio and processed through graph-based augmentations. This approach highlights the importance of increasing graph structure diversity during label-free pre-training, which facilitates the discovery of meaningful data representations and improving detection performance, particularly during fine-tuning.
- We conduct an extensive evaluation of SIGNAL on multiple audio deepfake datasets under limited label conditions. Our results demonstrate that SIGNAL outperforms state-of-the-art supervised audio deepfake detection models as well as contrastive and non-contrastive learning models for audio data. SIGNAL achieves the lowest Equal Error Rate (EER) with as little as 5% labeled data and exhibits strong generalization capabilities, consistently achieving the lowest EER in cross-domain evaluations involving different attack types and languages on the In-The-Wild dataset.

The rest of this paper is organized into the following sections. Section II provides an overview of related works,

including current GNNs for audio deepfake detection and contrastive learning on audio data. Section III explains the notations and the problem we aim to solve. Section IV presents the details of our SIGNAL for audio deepfake detection. We provide the experimental results and discussion in Section V and conclude this work in Section VI.

II. RELATED WORK

A. GNNs for Audio Deepfake Detection

Recent advancements show that GNNs outperform typical deep learning models for audio deepfake detection tasks [13], [14]. GNNs require a data management process where a visual representation of audio data, such as a spectrogram, is converted into graph structures. This is achieved by dividing it into patches and exploring interdependencies between components in frequency sub-bands or temporal segments. Some techniques like GAT-T [17] and RawGAT-ST [16] employ the ResNet model [11] to generate latent vectors treated as graph nodes and learn the graph structures using a graph attention network (GAT) [32]. AASIST [14] further improves these approaches by employing the heterogeneous stacking graph attention layer. Another technique by Chen et al. [13] uses spectrogram patches as nodes derived from linear filterbanks (LFB), with relationships between patches forming the edges and modeling it using a graph convolutional network (GCN) [33]. Recent advancements have introduced hybrid frameworks that combine self-supervised learning (SSL) methods, such as Wav2Vec2 [34] and Whisper [35], to generate learnable visual representations, which are then integrated with GNN-based classifiers [18], [19].

Despite their effectiveness, *these GNN techniques heavily rely on large amounts of labeled data* to produce diverse graph structures. This dependence can lead to overfitting and reduced performance when samples with labels are limited during model training. Several attempts to generate more labeled data based on audio data augmentation methods, such as adding background noise or converting codec types [23], are inadequate since they only work for raw audio and cannot be transferred directly to graph structures. Our work addresses these challenges by adopting a holistic approach that enables graph-based augmentations to produce more variations in graph views and develops graph non-contrastive learning to better learn graph representations of audio data, even with limited labeled data.

B. Contrastive Learning on Audio Data

Self-supervised learning (SSL) has gained attention for its ability to develop models without requiring labeled data [22]. Among SSL techniques, contrastive learning has emerged as a powerful approach to improve data representation by grouping similar data closely and separating dissimilar ones [22]. This is often achieved through augmentations that create diverse views of the input data. Several contrastive learning models in computer vision include SimCLR [36], MoCo [37], BYOL [26], and SimSiam [27]. SimCLR and MoCo rely on positive and negative pairs to learn meaningful representations, whereas

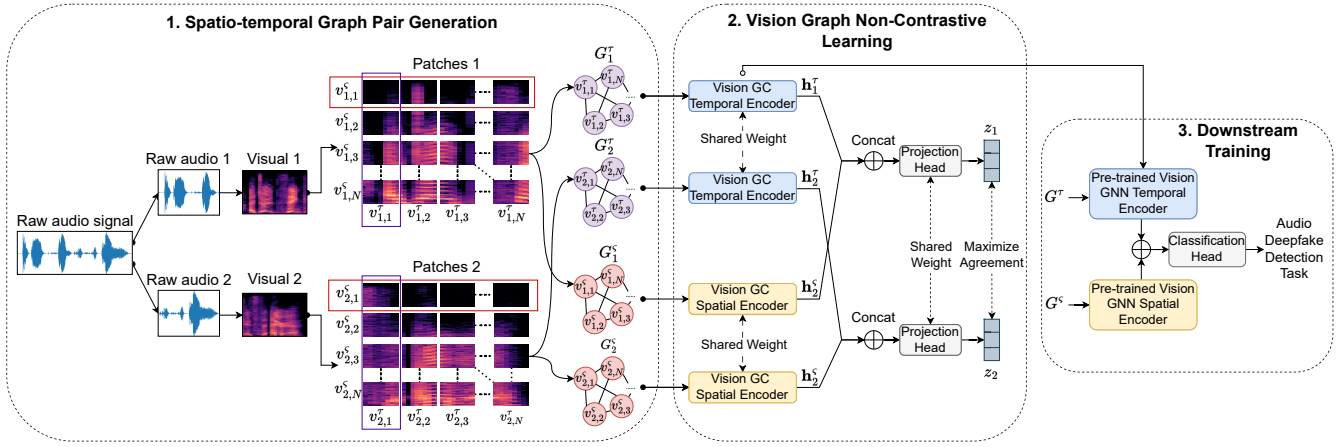


Fig. 1: The proposed SIGNAL framework. The SIGNAL starts with *spatio-temporal graph pair generation*, creating positive temporal and spatial graph pairs from audio data. Next, *vision graph non-contrastive learning* pre-trains vision GC encoders by minimizing the similarity between the positive pair without requiring annotated labels. Finally, *downstream task training* fine-tunes the pre-trained encoders to address audio deepfake detection, enabling the use of minimal labels.

methods like BYOL and SimSiam use only positive pairs, a technique known as non-contrastive learning [22].

Contrastive learning has been extended to audio data. For instance, SimCLR [36], initially designed for visual data, was adapted for audio by Zang et al. [38]. Similarly, MoCo [37] was repurposed as MoCo speaker embedding to learn speech representations [39]. COLA [40] employs contrastive learning to train models for universal audio understanding, while Wang et al. [41] introduced Angular Contrastive Loss (ACL) to enhance the discriminative power of audio contrastive learning. In the non-contrastive domain, BYOL-A [42] adapts BYOL for audio tasks, demonstrating the versatility of non-contrastive learning in the audio domain.

However, existing contrastive and non-contrastive learning methods operate on raw audio or visual forms, such as spectrograms, which are not well-suited for capturing knowledge of graph structures derived from the visual representation of audio. In contrast, our approach extends these methods to handle graph structures derived from the visual representation of audio by employing graph non-contrastive learning techniques [29], [30], which do not rely on negative samples. Moreover, unlike general audio contrastive learning approaches for audio, our framework is specifically designed for audio deepfake detection tasks. We aim to maintain the strengths of GNNs in scenarios with limited labeled data for audio deepfake detection tasks.

III. PRELIMINARIES

In this section, we first introduce basic concepts of managing graph structures derived from audio data and provide a high-level overview of our pre-trained vision graph convolution (GC) encoders used in audio deepfake detection. Additionally, we summarize commonly used notations in Table I.

Graph Data. In this work, a graph is formally defined as $G = (V, E, X)$ where $V = \{v_1, v_2, \dots, v_N\}$ represents a

TABLE I: Summary of Key Notations

Notations	Description
G	Graph with nodes V , edges E , features X
V	Set of nodes in a graph
E	Set of edges between nodes
X	Node feature matrix
$e_{i,j}$	Edge between nodes v_i and v_j
x_i	Feature vector for node v_i
t	Audio clip duration in seconds
F	Frequency dimension of audio's visual representation
T	Temporal dimension of audio's visual representation
G^T	Temporal graph
G^S	Spatial graph
f^T	Temporal graph encoder
f^S	Spatial graph encoder
$H^{(\ell)}$	Set of node embeddings in layer ℓ
$h^{(\ell)}$	A node embedding in layer ℓ
\mathbf{h}^T	Graph-level representation for temporal graph
\mathbf{h}^S	Graph-level representation for spatial graph
z	Vector representation of an audio
$s(z_1, z_2)$	Cosine similarity of representations z_1, z_2
g	Projection head for dimensional reduction
c	Classification head for the downstream task
y	Classification output
\mathcal{L}_{align}	Alignment loss for positive pairs
\mathcal{L}_{CE}	Cross-entropy loss for detection training

set of nodes in a graph with N nodes. For $i \neq j$ and $i, j \in \{1, 2, \dots, N\}$, each edge $e_{i,j} = (v_i, v_j) \in E$ indicates a relationship between two nodes. The feature vector $x_i \in X$ is associated with each node v_i , where $X \in \mathbb{R}^{N \times D}$, and D denotes the dimension of the feature vector.

Spatio-temporal Graphs of Audio. In SIGNAL, each iteration of non-contrastive learning generates two audio samples as positive pairs. Each sample is represented by two types of graphs: a temporal graph G^T and a spatial graph G^S . For the first audio sample, this produces temporal graph $G_1^T = (V_1^T, E_1^T, X_1^T)$ and spatial graph $G_1^S = (V_1^S, E_1^S, X_1^S)$, and

for the second audio sample, this produces temporal graph $G_2^\tau = (V_2^\tau, E_2^\tau, X_2^\tau)$ and spatial graph $G_2^s = (V_2^s, E_2^s, X_2^s)$, where the indices 1 or 2 denote the corresponding audio sample. Given the temporal graph $G_1^\tau = (V_1^\tau, E_1^\tau, X_1^\tau)$, $V_1^\tau = \{v_{1,1}^\tau, v_{1,2}^\tau, \dots, v_{1,N}^\tau\}$ represents the set of nodes from the temporal graph of audio sample 1, where N denotes the total number of nodes.

Pre-trained Vision GC Encoders. SIGNAL aims to produce pre-trained encoders through a graph non-contrastive learning mechanism. Two encoders are pre-trained: a vision GC temporal encoder f^τ that is trained on the input temporal graph pair G_1^τ and G_2^τ , and a vision GC spatial encoder f^s that is trained on the input spatial graph pair G_1^s and G_2^s . The pre-trained encoders f^τ and f^s are then fine-tuned for the downstream task of audio deepfake detection. This combination of encoders generates a generic representation z , which is passed through a classification head to produce a prediction: $y = 1$ for genuine (bona fide) audio or $y = 0$ for fake audio.

IV. METHODOLOGY

Our proposed SIGNAL framework for audio deepfake detection, as shown in Figure 1, consists of the following three main components: *spatio-temporal graph pair generation*, *vision graph non-contrastive learning*, and *downstream training*. In this section, we describe each component in detail.

A. Spatio-temporal Graph Pair Generation

This section explains the components of managing positive temporal and spatial graph pairs from audio data. The steps include generating positive pairs, converting audio data into a graph structure, and performing graph data augmentation.

Generating Positive Pairs of Audio. Our work adopts a non-contrastive learning approach, which excludes negative samples, distinguishing it from traditional contrastive learning methods. In contrastive frameworks such as COLA [40], treating other audio samples in the same batch as negative pairs can lead to unintended outcomes. Specifically, samples from the same class—such as *genuine* or *fake*—may be incorrectly pushed apart in the feature space due to the presence of false negatives [28]. Moreover, recent work by Guo et al. [29] suggests that negative pairs are unnecessary for graph contrastive learning for graph classification tasks and that comparable performance can be achieved without them.

To generate positive pairs of raw audio, we adopt a simple segmentation approach inspired by COLA [40]. This involves splitting the original audio into two segments of similar size, ensuring consistent positive pairs while enabling efficient processing. Each audio clip is standardized to a fixed duration of t seconds. For clips shorter than t , the audio is repeated to meet the required length, whereas longer clips are truncated. Positive pairs are then sampled from the same t second audio, producing two segments: audio sample 1 and audio sample 2, each with a duration of $\lfloor \frac{t}{2} \rfloor$ seconds. These segments are subsequently converted into visual representations, such as spectrograms, with dimensions $F \times T$, where F represents the frequency axis and T represents the temporal axis.

Converting Audio Pairs into Spatio-temporal Graphs. To convert audio data into a graph structure, we divide its visual representation, such as a spectrogram, into patches. A visual representation of size $F \times T$, where F represents the frequency axis, and T the temporal axis, is segmented into N patches along both the vertical (temporal segmentation) and horizontal (spatial segmentation) dimensions. Each temporal patch is transformed into a feature vector $x_i^\tau \in \mathbb{R}^D$, forming the overall feature matrix $X^\tau = [x_1^\tau, x_2^\tau, \dots, x_N^\tau]$. Similarly, each spatial patch is transformed into a feature vector $x_i^s \in \mathbb{R}^D$, with the overall feature matrix represented as $X^s = [x_1^s, x_2^s, \dots, x_N^s]$.

These feature vectors correspond to nodes, denoted as V^τ for temporal patches and V^s for spatial patches. For each node v_i in both views, we identify its K nearest neighbors $\mathcal{N}(v_i)$ and establish edges e_{ji} from neighboring nodes v_j to v_i for all $v_j \in \mathcal{N}(v_i)$. This process results in fully constructed spatio-temporal graphs $G^\tau = (V^\tau, E^\tau, X^\tau)$ for the temporal view and $G^s = (V^s, E^s, X^s)$ for the spatial view. Each step processes two audio samples as a positive pair, generating four graphs: G_1^τ and G_1^s for first audio sample, and G_2^τ and G_2^s for the second.

Graph-based Augmentations. This process modifies the spatio-temporal graphs in the positive pairs by dynamically introducing varied graph characteristics during the pre-training phase. Diversification of graph properties enables the model to better capture underlying structures, enhances robustness to noise, and improves generalization to unseen graph structures, thereby enhancing performance in downstream tasks [30]. Building on the work of Guo et al. [29], we employ three types of graph-based augmentations:

- **Edge Dropping (ED):** Randomly removes edges from the graph, increasing sparsity.
- **Gaussian Noise (GN):** Adds random noise sampled from a Gaussian distribution to the node features.
- **Feature Masking (FM):** Randomly sets a proportion of node features to zero.

The optimal combination of these graph augmentations is analyzed in subsection V-E.

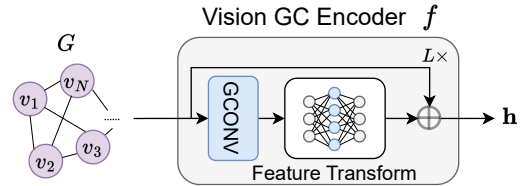


Fig. 2: Vision GC Encoder.

B. Vision Graph Non-Contrastive Learning

This section introduces our vision graph non-contrastive learning module, which processes positive temporal and spatial graph pairs. This module enables the pre-training process to learn graph representations without labels by maximizing the similarity between positive graph pairs.

Vision Graph Convolution Encoder. The Vision graph convolution (GC) encoder, inspired by Vision GNN [15], was originally developed for image classification and object detection tasks. We use the term “vision” in this work because we model the visual representation of audio, such as spectrograms or other 2D matrices that can be visualized as heatmaps. We further extend this technique to make it suitable for processing audio data. After deriving graph structures from the audio, each graph G is processed through the vision GC encoder. The GNNs model graph representation by enabling nodes to exchange information through feature aggregation from their neighbors, where nodes represent patches in the audio’s visual representation.

The proposed vision GC encoder is depicted in Figure 2. This encoder models a graph G through a function defined as vision GC f , producing an output \mathbf{h} , expressed as $f(G) \rightarrow \mathbf{h}$. For the encoder’s first component, we employ a graph convolution network (GCN) [33] due to its simplicity and efficiency. The GCN layer is defined as follows:

$$H^{(\ell+1)} = \sigma(\hat{D}^{-\frac{1}{2}} \hat{A} \hat{D}^{-\frac{1}{2}} H^{(\ell)} \theta^{(\ell)}), \quad (1)$$

where $H^{(\ell+1)}$ is the set of updated node embeddings, and $H^{(\ell)}$ represents the node embeddings from the previous layer. The initial node embeddings H^0 correspond to the original node feature matrix X of graph G . Here $\hat{A} = A + I$ denotes the adjacency matrix with self-loops, \hat{D} is the diagonal degree matrix of \hat{A} , and $\theta^{(\ell)}$ are the learnable parameters of layer ℓ . The function $\sigma(\cdot)$ is a nonlinear activation function (e.g., ReLU).

We implement the multi-head operation as a *feature transformation module* to enhance the expressiveness of node embeddings after graph convolution. The transformation involves splitting the feature embedding of each node $h_i^{(\ell+1)}$ into K heads: $head_1, head_2, \dots, head_K$. Each head projects the node representation using different weights. The feature embeddings from all heads are updated in parallel, and their results are concatenated to form the updated feature vector:

$$\begin{aligned} h_i^{(\ell+1)} &= \parallel_{j=1}^K head_j \theta_j \\ &= [head_1 \theta_1 \parallel head_2 \theta_2 \parallel \dots \parallel head_K \theta_K]. \end{aligned} \quad (2)$$

This multi-head operation improves the model’s feature diversity. To address the vanishing gradient problem, we incorporate a skip connection in each layer of the GNN encoder. The updated feature embedding of each node, which combines the skip connection with the multi-head operation, is given by $h_i^{(\ell+1)} = \sigma(h_i^{(\ell+1)}) + h_i^{(\ell)}$, where $\sigma(\cdot)$ denotes an activation function (e.g., ReLU), and $h_i^{(\ell)}$ represents the node’s previous representation before the GCN operation.

In this study, the node embeddings H after ℓ layers of convolution are concatenated to form the graph-level representation by aggregating nodes. For each graph, CONCAT pooling is performed as follows:

$$\mathbf{h} = \parallel_{j=1}^N h_j = [h_1 \parallel h_2 \parallel \dots \parallel h_N]. \quad (3)$$

During the vision graph non-contrastive learning process, we pre-train two encoders through an unsupervised, label-free mechanism. The temporal encoder f^τ is trained on the temporal graph pair G_1^τ and G_2^τ using shared weights, meaning the same encoder is applied to both graphs. Similarly, the spatial encoder f^s is trained separately on the spatial graph pair G_1^s and G_2^s , also with shared weights.

Projection Head. Each audio sample in the positive pair generates spatio-temporal graph representations: \mathbf{h}^τ for the temporal graph and \mathbf{h}^s for the spatial graph. These representations are combined into a single vector using a projection head g , which takes the concatenation of \mathbf{h}^τ and \mathbf{h}^s as input and reduces the dimensionality to produce a vector representation $z = g(\mathbf{h}^\tau \parallel \mathbf{h}^s)$. This process yields two vectors for the positive pair: z_1 for audio sample 1 and z_2 for audio sample 2. The projection head is implemented as a simple multi-layer perceptron with shared weights, applied identically to both positive samples.

Algorithm 1 Vision Non-Graph Contrastive Learning.

Require: Training Data $\mathcal{D} = \{(G_1^\tau, G_1^s, G_2^\tau, G_2^s)\}_{i=1}^M$, number of epochs Ep, batch size Bt.

Ensure: Pre-trained GNN encoders f^τ and f^s .

- 1: **Parameters:** Temporal GNN encoder f_θ^τ , Spatial GNN encoder f_θ^s , projection head g_ϕ
 - 2: **for** epoch = 1 to Ep **do**
 - 3: **for** each batch $\{(G_1^\tau, G_1^s, G_2^\tau, G_2^s)\}$ of size Bt from \mathcal{D} **do**
 - 4: $G_1^\tau \leftarrow \text{Augment}(G_1^\tau)$ {Augment each G_1^τ in the batch}
 - 5: $G_1^s \leftarrow \text{Augment}(G_1^s)$ {Augment each G_1^s in the batch}
 - 6: $G_2^\tau \leftarrow \text{Augment}(G_2^\tau)$ {Augment each G_2^τ in the batch}
 - 7: $G_2^s \leftarrow \text{Augment}(G_2^s)$ {Augment each G_2^s in the batch}
 - 8: $\mathbf{h}_1^\tau \leftarrow f_\theta^\tau(G_1^\tau)$ {Apply encoder to the graph G_1^τ }
 - 9: $\mathbf{h}_1^s \leftarrow f_\theta^s(G_1^s)$ {Apply encoder to the graph G_1^s }
 - 10: $\mathbf{h}_2^\tau \leftarrow f_\theta^\tau(G_2^\tau)$ {Apply encoder to the graph G_2^τ }
 - 11: $\mathbf{h}_2^s \leftarrow f_\theta^s(G_2^s)$ {Apply encoder to the graph G_2^s }
 - 12: $z_1 \leftarrow g_\phi(\mathbf{h}_1^\tau \parallel \mathbf{h}_1^s)$ {Project embeddings of the anchor}
 - 13: $z_2 \leftarrow g_\phi(\mathbf{h}_2^\tau \parallel \mathbf{h}_2^s)$ {Project embeddings of the positive}
 - 14: $\mathcal{L}_{align} \leftarrow \mathcal{L}_{align}(z_1, z_2)$ {Calculate the loss}
 - 15: Update $\theta^\tau, \theta^s, \phi$ to minimize \mathcal{L}_{align} {Backpropagation}
 - 16: **end for**
 - 17: **end for**
 - 18: **return** $f_\theta^\tau, f_\theta^s$ {Return the pre-trained encoders}
-

Alignment Loss. In contrastive learning, the InfoNCE loss [43] is typically used to bring positive samples closer together and separate negative samples. However, since our framework consists only of positive pairs, we adopt the alignment component of the InfoNCE loss, denoted as $\mathcal{L}_{align}(z_1, z_2)$. This approach focuses exclusively on maximizing the agreement between positive pairs. Given a positive pair of vector representations z_1 and z_2 , the alignment loss is defined as:

$$\mathcal{L}_{align}(z_1, z_2) = - \sum \frac{s(z_1, z_2)}{t}, \quad (4)$$

where $s(z_1, z_2) = \frac{z_1^\top z_2}{\|z_1\| \|z_2\|}$ is the cosine similarity between the positive samples, and t is a temperature parameter that scales the similarity scores. Optimizing this loss increases the

similarity for positive pairs. The complete algorithm for spatio-temporal vision graph non-contrastive learning is described in Algorithm 1.

It is important to note that optimizing for positive similarity can result in the projection head g learning constant features for both z_1 and z_2 , a phenomenon known as feature collapse [29]. However, while the projection head g may exhibit collapse, the vision GC encoders remain unaffected. The projection head g introduces a non-linear transformation, ensuring that the encoders learn informative and distinct features [29]. Consequently, the pre-trained Vision GC encoders are effectively transferable for downstream tasks. Feature collapse is further discussed in subsection V-E.

C. Downstream Training

Downstream training fine-tunes the pre-trained encoders for the audio deepfake detection task, addressing scenarios with *limited labeled data*. Unlike a fixed approach that keeps parameters unchanged, we use a fine-tuning strategy to slightly adjust these encoder parameters for the new task. A comparison of the fixed and fine-tuning approaches is provided in subsection V-F.

Similar to pre-training, downstream training uses temporal and spatial graphs, denoted as G^T and G^S , derived from the audio data. These graphs are input to the pre-trained temporal GNN encoder f^T and spatial GNN encoder f^S . However, in the downstream training, the projection head g is replaced with a classification head c , which avoids the potential issue of collapsed features generated by g . The classification head c , implemented as a multi-layer perceptron, is designed to adapt to the audio detection task.

The graph-level representation \mathbf{h}^T and \mathbf{h}^S produced from the pre-trained temporal and spatial GNN encoders, are concatenated and passed to the classification head c to obtain the final prediction:

$$y = c(\mathbf{h}^T \parallel \mathbf{h}^S), \quad (5)$$

where $y = 1$ indicates genuine (bona fide) audio, and $y = 0$ indicates fake audio. Downstream training minimizes the cross-entropy loss $\mathcal{L}_{CE}(y, \hat{y})$, where y is the predicted label, and \hat{y} is the true label. The loss function is defined as:

$$\mathcal{L}_{CE}(y, \hat{y}) = - \sum_{i=1}^C \hat{y}_i \log(y_i), \quad (6)$$

where $C = 2$ represents the number of classes: bona fide and fake. The complete algorithm for downstream training is described in Algorithm 2.

V. EXPERIMENTS

In this section, we evaluate SIGNAL through experiments designed to answer the following research questions:

- **RQ1:** Can SIGNAL outperform existing baselines in both *in-domain* evaluation, where the training and evaluation sets originate from similar audio deepfake dataset sources, and *cross-domain* evaluation, where the training

Algorithm 2 Downstream Training.

Require: Training Data $\mathcal{D} = \{(G^T, G^S, \hat{y})\}_{i=1}^M$ with labels, number of epochs Ep, batch size Bt.

Ensure: Trained model for audio deepfake detection tasks.

```

1: Parameter: Classification head  $c_\phi$ .
2: Load parameters for  $f_\theta^T$  and  $f_\theta^S$  from pre-trained models
3: for epoch = 1 to Ep do
4:   for each batch  $\{(G^T, G^S, \hat{y})\}$  of size Bt from  $\mathcal{D}$  do
5:      $\mathbf{h}^T \leftarrow f_\theta^T(G^T)$  {Apply encoder to each  $G^T$  in the batch}
6:      $\mathbf{h}^S \leftarrow f_\theta^S(G^S)$  {Apply encoder to each  $G^S$  in the batch}
7:      $y \leftarrow c_\phi(\mathbf{h}^T \parallel \mathbf{h}^S)$  {Concatenate and classify embeddings}
8:      $\mathcal{L}_{CE} \leftarrow \mathcal{L}_{CE}(y, \hat{y})$  {Calculate the batch loss}
9:     Update  $\theta^T, \theta^S, \phi$  to minimize  $\mathcal{L}_{CE}$  {Backpropagation}
10:  end for
11: end for
12: return  $f_\theta^T, f_\theta^S, c_\phi$  {Return the trained model}

```

and evaluation sets come from different dataset sources, even with *limited labeled data*?

- **RQ2:** Do the three combinations of graph augmentations contribute significantly to SIGNAL’s performance?
- **RQ3:** What is the impact of each module in SIGNAL on improving audio deepfake detection?
- **RQ4:** How does SIGNAL’s performance vary with different settings of key parameters?

A. Datasets and evaluation metric

We evaluate SIGNAL and baseline methods using the ASVspoof 2021 DF [23], the newly released ASVspoof 5 [44], and the Chinese fake audio detection (CFAD) [45] datasets under different limited data scenarios. We additionally use the In-The-Wild [46] dataset to assess performance on unseen data distributions.

ASVspoof 2021 DF: We use the evaluation set from the deepfake (DF) track, which focuses on audio deepfake detection under realistic conditions. The dataset contains bona fide and fake speech processed through various audio codecs. Its training and development sets are sourced from the logical access (LA) track of ASVspoof 2019 [47], featuring fake audio generated through speech synthesis and voice conversion techniques.

ASVspoof 5: The latest ASVspoof challenge dataset includes crowdsourced data with diverse acoustic conditions. We use its training and development sets, which include both bona fide and attack samples. The training set contains attacks A01–A08, while the development set contains attacks A09–A16. Since the official test set labels have not yet been released, we simulate a test set by splitting the development set into two parts: one for validation (containing A09–A14) and another for evaluation (A09–A14 with additional unseen attacks, A15 and A16).

CFAD: The Chinese Fake Audio Detection (CFAD) dataset features Chinese speakers and includes four subsets: training, development, seen test, and unseen test. The unseen test contains new attack types and scenarios to evaluate model generalization. For our experiments, we combine the seen and unseen test subsets into a unified test set.

TABLE II: Statistics for training (train), development (dev), and evaluation (eval) sets across datasets.

Set	ASVspoof 2021 DF (English)			ASVspoof5 (English)			CFAD (Chinese)			In-The-Wild (English)		
	Bona fide	Fake	Total	Bona fide	Fake	Total	Bona fide	Fake	Total	Bona fide	Fake	Total
Train	2,580	22,800	25,380	18,797	163,560	182,357	12,800	25,600	38,400	-	-	-
Dev	2,548	22,296	24,844	15,667	41,106	56,773	4,800	9,600	14,400	-	-	-
Eval	22,617	589,211	611,828	15,667	68,510	84,177	21,000	42,000	63,000	19,963	11,816	31,779

In-The-Wild: To evaluate robustness in unseen scenarios, we perform cross-domain evaluations using the In-the-Wild dataset [46], which includes audio deepfakes of politicians and public figures collected from platforms like video streaming and social media. Dataset statistics are summarized in II.

Notably, we avoid using extensive raw audio augmentations such as codec conversion, reverberation, background noise addition, high- and low-pass filtering, and Raw Boost, commonly employed in prior frameworks. Instead, our experiments focus on *limited label scenarios* using the original unprocessed data without to ensure a fair comparison between our framework and the baselines under consistent conditions.

EER Metric: Performance is measured using the **equal error rate (EER)**, a standard metric in biometric systems. A lower EER indicates better performance in distinguishing bona fide from fake audio samples.

B. Experimental Settings

Each audio clip was processed to a uniform length of $t = 9$ seconds. Shorter audio clips were repeated to meet this duration, while longer clips were trimmed. During pre-training, each positive pair consisted of two 4.5-second segments randomly extracted from the 9-second audios. In downstream training, only 4.5-second audio segments were used as inputs.

To transform raw audio data into a 2D matrix, we used Wav2Vec2 [34], a pre-trained SSL model for automatic speech recognition (ASR). Specifically, the wav2vec2-xls-r-300m variant was employed to generate feature matrices serving as visual representations of the audio, fine-tuned for audio deepfake detection tasks. Each resulting 2D matrix had dimensions of (1024, 224). These matrices were divided into 32 temporal and 32 spatial patches, resulting in two graph views (temporal and spatial) with 32 nodes each across all datasets. During model training, we utilized a *k-nearest neighbors* graph with three outgoing edges per node for ASVspoof 2021 DF and ASVspoof 5, and four for CFAD. Details on parameter sensitivity are provided in subsection V-G.

Experiments were conducted on an Intel Xeon Platinum 8452Y 3.20 GHz processor and an NVIDIA H100 GPU. Visual representations were processed into patches (nodes) through a *stem convolutional layer* [15] before being passed into the vision GC encoders. Each node had a 256-dimensional feature vector. The vision GC encoders consisted of a 5-layer pyramid architecture for both temporal and spatial graph processing, halving the embedding size at each layer. A 3-layer projection head with 256, 128, and 80 hidden dimensions was used during pre-training, which was later replaced by a classifier head with similar dimensions for the audio deepfake detection task.

Training was performed with a batch size of 96 using the Adam optimizer. The learning rates were set to 0.00001 for ASVspoof 2021 DF and ASVspoof 5, and 0.0001 for CFAD. Both pre-training and downstream training ran for 100 epochs with early stopping criteria applied.

C. Baseline Models

The baselines were categorized into two groups. The first category included standard supervised models for audio deepfake detection, such as LCNN [9], which uses Linear Frequency Cepstral Coefficients (LFCC) as input, and AASIST [14], an enhanced graph-based model built on GAT-T [17] and RawGAT-ST [16], which process raw audio directly. We also evaluated supervised methods leveraging learnable audio representations from SSL models like Wav2Vec2 [34] and Whisper [35], fine-tuned for deepfake detection, as seen in recent state-of-the-art approaches [18], [48].

The second category included recent contrastive and non-contrastive learning techniques for audio, such as COLA [40], SimCLR [38], BYOL-A [42], MoCo [39], and SSL-ACL [41]. These baselines were implemented using their official codebases, with optimal hyperparameters selected. Each model used its preferred audio data input type (*front-end*), and contrastive learning-based data augmentations as specified in their original implementations.

D. (RQ1) Comparison with Baseline Methods

To address RQ1, each model was evaluated under varying levels of label availability: 5%, 10%, 30%, 50%, 80%, and the full label set. These labelled subsets applied exclusively to the training and development sets, while the test set always retained the complete dataset information. In the limited label scenarios, the original proportional distribution of bona fide and fake samples, as well as the diversity of attack types, was preserved to reflect the composition of the complete training set. This approach ensures consistency in sample selection, reduces potential biases, and facilitates fair comparisons across all baseline methods. The number of labels available for the train and dev sets is summarized in Table V.

In-domain Evaluation Results. The results, summarized in Table III, show that SIGNL consistently outperforms other methods, achieving the lowest EER in in-domain evaluations across three datasets: ASVspoof 2021 DF, ASVspoof 5, and CFAD. In the full-label scenario, SIGNL achieves mean EERs of 7.21%, 2.33%, and 8.44% on ASVspoof 2021 DF, ASVspoof 5, and CFAD, respectively, surpassing all competing approaches. These results highlight SIGNL’s strong capability in detecting audio deepfakes when full labeled

TABLE III: EER (%) comparison across different training label percentages for in-domain evaluation. All values represent mean \pm standard deviation. Lower values: better performance (\downarrow). **Bold**: best result.

Categories	Methods	Front-end	ASVspoof 2021 DF					
			5%	10%	30%	50%	80%	Full
Supervised	LCNN	LFCC	30.26 \pm 2.03	28.91 \pm 2.57	25.63 \pm 0.46	25.99 \pm 0.72	25.21 \pm 0.45	25.44 \pm 0.82
	LCNN	Whisper	24.61 \pm 4.35	18.09 \pm 1.85	23.49 \pm 8.63	19.38 \pm 2.43	20.32 \pm 4.05	20.64 \pm 5.90
	LCNN	Wav2Vec2	38.42 \pm 5.24	28.52 \pm 7.56	9.36 \pm 2.79	11.90 \pm 3.90	8.63 \pm 0.93	12.16 \pm 3.06
	AASIST	Raw Waveform	25.45 \pm 3.88	23.72 \pm 1.15	22.79 \pm 1.76	22.78 \pm 2.41	22.48 \pm 1.33	22.85 \pm 1.52
	AASIST	Whisper	14.87 \pm 1.19	14.55 \pm 0.99	13.31 \pm 0.47	14.06 \pm 0.64	14.40 \pm 1.05	16.48 \pm 1.66
	AASIST	Wav2Vec2	28.81 \pm 8.72	8.47 \pm 0.70	8.65 \pm 1.58	8.60 \pm 0.86	8.92 \pm 1.34	9.26 \pm 1.38
Audio Contrastive/ Non-contrastive	SSL-ACL	Log-mel	35.77 \pm 1.57	31.94 \pm 0.56	27.42 \pm 1.02	26.36 \pm 1.02	26.05 \pm 0.38	26.00 \pm 0.53
	BYOL-A	Log-mel	23.55 \pm 0.63	22.08 \pm 0.74	22.92 \pm 0.18	21.69 \pm 0.79	21.91 \pm 0.81	21.77 \pm 0.13
	COLA	Log-mel	27.25 \pm 1.40	25.49 \pm 1.70	23.85 \pm 1.02	23.29 \pm 0.16	23.17 \pm 0.23	23.93 \pm 0.39
	MoCo	MFCC	27.89 \pm 1.15	28.35 \pm 0.84	28.90 \pm 0.76	28.45 \pm 1.57	28.08 \pm 0.40	26.99 \pm 1.12
	SimCLR	Log-mel	24.95 \pm 1.18	24.72 \pm 1.13	22.64 \pm 0.62	20.92 \pm 1.60	20.92 \pm 0.77	20.47 \pm 0.70
	SIGNL	Wav2Vec2	7.88 \pm 2.11	6.76 \pm 1.05	6.85 \pm 0.36	7.01 \pm 1.40	6.51 \pm 0.52	7.21 \pm 0.61

Categories	Methods	Front-end	ASVspoof 5					
			5%	10%	30%	50%	80%	Full
Supervised	LCNN	LFCC	25.06 \pm 1.88	22.07 \pm 3.53	19.40 \pm 0.32	17.29 \pm 0.23	17.25 \pm 1.08	17.65 \pm 1.18
	LCNN	Whisper	20.70 \pm 0.58	19.08 \pm 0.10	16.82 \pm 5.02	19.37 \pm 0.14	17.61 \pm 1.40	18.86 \pm 1.94
	LCNN	Wav2Vec2	15.89 \pm 4.61	11.77 \pm 4.31	5.74 \pm 2.91	4.15 \pm 2.14	3.85 \pm 0.91	5.92 \pm 0.69
	AASIST	Raw Waveform	31.41 \pm 8.78	22.96 \pm 0.10	25.29 \pm 3.44	20.21 \pm 1.29	21.48 \pm 3.01	22.37 \pm 0.95
	AASIST	Whisper	21.91 \pm 6.84	18.60 \pm 6.23	19.05 \pm 5.92	14.31 \pm 1.27	11.81 \pm 2.78	16.32 \pm 4.92
	AASIST	Wav2Vec2	6.83 \pm 2.68	6.91 \pm 1.99	4.91 \pm 2.93	10.34 \pm 2.63	3.05 \pm 1.17	3.00 \pm 0.76
Audio Contrastive/ Non-contrastive	SSL-ACL	Log-mel	18.70 \pm 0.33	17.15 \pm 0.15	15.24 \pm 0.13	15.00 \pm 0.48	14.20 \pm 0.37	13.95 \pm 1.13
	BYOL-A	Log-mel	16.19 \pm 1.64	18.72 \pm 1.97	14.94 \pm 2.89	16.75 \pm 2.79	14.57 \pm 2.06	13.40 \pm 2.25
	COLA	Log-mel	14.71 \pm 1.16	14.63 \pm 1.14	14.17 \pm 0.21	14.47 \pm 0.82	13.52 \pm 0.84	13.43 \pm 1.07
	MoCo	MFCC	30.59 \pm 0.82	29.94 \pm 0.56	26.59 \pm 1.88	25.65 \pm 0.99	24.93 \pm 0.38	24.53 \pm 1.78
	SimCLR	Log-mel	17.51 \pm 1.03	15.22 \pm 1.58	16.29 \pm 1.83	15.71 \pm 2.14	13.49 \pm 0.72	12.78 \pm 1.93
	SIGNL	Wav2Vec2	3.95 \pm 1.34	2.43 \pm 0.88	2.86 \pm 1.30	2.65 \pm 1.21	1.89 \pm 0.97	2.33 \pm 0.66

Categories	Methods	Front-end	CFAD					
			5%	10%	30%	50%	80%	Full
Supervised	LCNN	LFCC	25.42 \pm 0.50	24.94 \pm 1.82	22.14 \pm 2.44	22.36 \pm 0.76	20.87 \pm 0.54	20.02 \pm 2.18
	LCNN	Whisper	16.58 \pm 2.08	16.73 \pm 2.23	13.19 \pm 0.48	12.46 \pm 0.77	11.32 \pm 0.66	10.52 \pm 0.50
	LCNN	Wav2Vec2	10.38 \pm 0.08	11.19 \pm 1.81	11.33 \pm 1.26	8.71 \pm 0.39	9.64 \pm 0.01	9.09 \pm 0.55
	AASIST	Raw Waveform	29.55 \pm 2.06	23.45 \pm 1.69	18.33 \pm 0.83	17.62 \pm 0.34	17.76 \pm 0.87	17.04 \pm 0.21
	AASIST	Whisper	16.72 \pm 2.60	14.99 \pm 1.29	13.39 \pm 0.54	12.28 \pm 0.17	12.74 \pm 1.10	12.47 \pm 0.93
	AASIST	Wav2Vec2	11.96 \pm 3.22	12.04 \pm 3.08	9.80 \pm 0.58	9.76 \pm 1.20	9.11 \pm 0.40	8.83 \pm 0.52
Audio Contrastive/ Non-contrastive	SSL-ACL	Log-mel	29.44 \pm 0.37	36.20 \pm 0.58	33.47 \pm 0.47	31.59 \pm 0.32	30.67 \pm 0.24	29.14 \pm 0.85
	BYOL-A	Log-mel	21.94 \pm 2.10	20.32 \pm 3.17	16.81 \pm 1.60	16.19 \pm 1.09	16.68 \pm 0.43	15.84 \pm 0.90
	COLA	Log-mel	21.14 \pm 0.10	21.48 \pm 0.75	18.44 \pm 0.62	18.70 \pm 0.20	16.45 \pm 1.46	18.52 \pm 1.30
	MoCo	MFCC	28.59 \pm 1.07	24.00 \pm 1.60	22.92 \pm 1.59	20.96 \pm 1.46	20.39 \pm 1.55	20.10 \pm 0.61
	SimCLR	Log-mel	27.23 \pm 1.01	20.94 \pm 1.11	20.50 \pm 0.49	17.56 \pm 1.02	17.59 \pm 0.81	16.87 \pm 0.36
	SIGNL	Wav2Vec2	9.90 \pm 0.20	8.84 \pm 0.10	8.77 \pm 0.20	8.46 \pm 0.21	8.83 \pm 0.50	8.44 \pm 0.12

data is available. *Even with limited labeled data*, SIGNL remains highly effective. With just 5% of labeled data, it achieves mean EERs of 7.88% on ASVspoof 2021 DF, 3.95% on ASVspoof 5, and 9.90% on CFAD, outperforming all baseline competitors. Notably, SIGNL sometimes performs better with smaller label percentages, likely because smaller labeled subsets reduce noise, providing better data quality and enabling more effective knowledge discovery.

SIGNL consistently outperforms supervised models like LCNN and AASIST, even when these models use different front-end configurations. This demonstrates SIGNL’s ability to leverage non-contrastive learning for extracting meaningful audio representations without heavily relying on labeled data during pre-training. By transforming audio data into spatio-temporal graphs and applying diverse graph-based augmentations, SIGNL enhances input variability and effectively clusters positive samples. This allows the model to learn rich, generalizable features during pre-training, which it fine-tunes

for downstream tasks. In contrast, supervised models like LCNN and AASIST struggle in low-label scenarios, showing rising EERs when only 5% of labeled data is available.

Additionally, SIGNL also surpasses contrastive and non-contrastive baselines, including SSL-ACL, BYOL-A, COLA, MoCo, and SimCLR. Its superior performance stems from its graph-based representations, which capture complex relationships between frequency sub-bands and temporal segments. This enables SIGNL to more accurately identify synthetic artifacts dispersed across the visual representation of audio. The combination of graph-based learning and non-contrastive pre-training ensures robust detection, even with limited label data, making SIGNL a powerful solution for audio deepfake detection.

Cross-domain Evaluation Results. To evaluate generalization, we tested SIGNL and baseline methods on the In-The-Wild dataset, focusing on their ability to handle diverse audio deepfake attacks in out-of-domain scenarios. This evaluation

TABLE IV: EER (%) comparison across different levels of label information for cross-domain evaluation on In-The-Wild dataset. All values represent mean \pm standard deviation. Lower values: better performance (\downarrow). **Bold**: best result.

Categories	Methods	Front-end	Trained on ASVspoof 2021 DF, Tested on In-The-Wild					
			5%	10%	30%	50%	80%	Full
Supervised	LCNN	LFCC	51.04 \pm 5.33	48.36 \pm 1.47	50.09 \pm 2.88	49.67 \pm 0.80	49.37 \pm 3.66	47.90 \pm 1.48
	LCNN	Whisper	33.78 \pm 2.67	29.19 \pm 5.36	26.98 \pm 2.76	30.03 \pm 4.06	27.97 \pm 2.43	28.56 \pm 5.18
	LCNN	Wav2Vec2	39.44 \pm 1.54	32.01 \pm 9.96	33.16 \pm 0.33	27.12 \pm 2.03	18.85 \pm 0.75	14.43 \pm 5.53
	AASIST	Raw Waveform	45.92 \pm 3.31	41.91 \pm 4.90	45.10 \pm 6.46	45.96 \pm 5.36	47.33 \pm 3.48	48.57 \pm 3.90
	AASIST	Whisper	30.45 \pm 1.40	29.19 \pm 0.49	28.19 \pm 2.06	28.85 \pm 1.00	27.64 \pm 1.80	28.29 \pm 3.27
Audio Contrastive/ Non-contrastive	AASIST	Wav2Vec2	36.16 \pm 6.08	18.71 \pm 4.48	13.96 \pm 1.79	12.20 \pm 2.82	16.06 \pm 3.94	12.68 \pm 3.50
	SSL-ACL	Log-mel	53.13 \pm 1.78	57.03 \pm 1.56	66.37 \pm 6.15	73.85 \pm 1.61	75.58 \pm 4.56	76.89 \pm 0.99
	BYOL-A	Log-mel	59.75 \pm 5.87	63.18 \pm 6.60	66.24 \pm 1.72	69.41 \pm 7.12	69.63 \pm 2.97	70.47 \pm 3.81
	COLA	Log-mel	56.42 \pm 8.77	65.34 \pm 3.93	74.62 \pm 5.24	78.89 \pm 2.31	77.00 \pm 5.39	76.61 \pm 0.14
	MoCo	MFCC	59.91 \pm 4.84	57.62 \pm 8.77	55.09 \pm 4.29	53.55 \pm 5.49	64.43 \pm 0.83	52.43 \pm 0.33
SimCLR	Log-mel	38.15 \pm 4.30	41.52 \pm 3.37	36.09 \pm 5.27	33.36 \pm 7.47	28.79 \pm 1.37	30.08 \pm 2.49	
	SIGNL	Wav2Vec2	14.85 \pm 2.21	12.51 \pm 0.50	10.18 \pm 1.43	9.67 \pm 1.55	11.18 \pm 1.50	10.89 \pm 3.10

Categories	Methods	Front-end	Trained on ASVspoof 5, Tested on In-The-Wild					
			5%	10%	30%	50%	80%	Full
Supervised	LCNN	LFCC	46.26 \pm 1.21	49.58 \pm 1.38	52.79 \pm 1.77	51.68 \pm 2.46	51.89 \pm 3.08	53.46 \pm 1.17
	LCNN	Whisper	33.78 \pm 3.28	29.19 \pm 6.56	26.98 \pm 3.38	30.03 \pm 4.97	27.97 \pm 2.97	28.56 \pm 6.34
	LCNN	Wav2Vec2	37.33 \pm 4.10	42.64 \pm 3.67	30.76 \pm 1.07	36.21 \pm 5.97	29.16 \pm 5.02	32.71 \pm 5.02
	AASIST	Raw Waveform	34.93 \pm 3.91	29.51 \pm 2.06	26.91 \pm 0.59	26.73 \pm 1.46	25.56 \pm 2.03	26.86 \pm 2.10
	AASIST	Whisper	32.91 \pm 7.97	31.05 \pm 3.91	29.62 \pm 2.41	26.54 \pm 2.06	24.86 \pm 3.99	24.59 \pm 3.19
Audio Contrastive/ Non-contrastive	AASIST	Wav2Vec2	37.48 \pm 2.06	39.29 \pm 7.22	36.11 \pm 6.92	46.32 \pm 3.76	28.10 \pm 1.94	31.88 \pm 3.84
	SSL-ACL	Log-mel	78.87 \pm 1.27	77.71 \pm 0.12	71.55 \pm 0.59	71.18 \pm 1.66	68.42 \pm 2.40	71.43 \pm 3.41
	BYOL-A	Log-mel	79.27 \pm 2.91	77.12 \pm 5.02	76.73 \pm 3.03	73.73 \pm 3.28	75.25 \pm 1.97	73.72 \pm 1.65
	COLA	Log-mel	68.57 \pm 2.56	75.95 \pm 7.81	75.24 \pm 3.93	78.22 \pm 1.32	76.35 \pm 4.00	71.74 \pm 2.64
	MoCo	MFCC	55.02 \pm 3.07	65.81 \pm 3.12	54.78 \pm 2.79	74.98 \pm 4.36	69.11 \pm 0.10	69.56 \pm 4.11
SimCLR	Log-mel	39.96 \pm 2.52	45.97 \pm 5.74	45.62 \pm 5.79	39.46 \pm 0.51	56.59 \pm 1.50	52.24 \pm 2.46	
	SIGNL	Wav2Vec2	31.72 \pm 2.59	27.62 \pm 4.46	28.66 \pm 3.57	24.24 \pm 5.15	22.99 \pm 2.41	27.43 \pm 2.29

Categories	Methods	Front-end	Trained on CFAD, Tested on In-The-Wild					
			5%	10%	30%	50%	80%	Full
Supervised	LCNN	LFCC	48.39 \pm 2.61	53.69 \pm 3.08	56.51 \pm 1.11	58.37 \pm 1.71	60.02 \pm 2.89	56.83 \pm 2.44
	LCNN	Whisper	47.61 \pm 2.80	47.89 \pm 2.91	43.64 \pm 2.16	46.29 \pm 2.70	47.92 \pm 0.44	48.73 \pm 1.26
	LCNN	Wav2Vec2	13.04 \pm 2.90	15.03 \pm 0.80	13.27 \pm 4.01	8.16 \pm 0.16	8.91 \pm 0.74	8.35 \pm 2.05
	AASIST	Raw Waveform	56.12 \pm 6.95	57.16 \pm 1.38	57.06 \pm 6.31	62.22 \pm 0.28	56.89 \pm 5.43	60.60 \pm 4.39
	AASIST	Whisper	44.03 \pm 6.48	47.66 \pm 3.76	48.58 \pm 2.21	50.08 \pm 3.46	49.80 \pm 2.96	48.66 \pm 0.65
Audio Contrastive/ Non-contrastive	AASIST	Wav2Vec2	13.74 \pm 1.85	13.06 \pm 3.05	9.74 \pm 2.56	10.23 \pm 0.40	10.12 \pm 3.52	11.35 \pm 0.93
	SSL-ACL	Log-mel	71.97 \pm 3.25	71.12 \pm 0.19	72.31 \pm 1.46	69.19 \pm 0.33	69.71 \pm 0.62	73.22 \pm 3.89
	BYOL-A	Log-mel	65.58 \pm 6.50	68.18 \pm 4.67	69.98 \pm 3.27	70.89 \pm 3.17	71.54 \pm 5.39	71.42 \pm 2.57
	COLA	Log-mel	70.52 \pm 0.43	71.77 \pm 0.96	69.53 \pm 0.73	70.17 \pm 1.15	68.35 \pm 2.00	61.79 \pm 4.47
	MoCo	MFCC	64.05 \pm 6.27	64.70 \pm 4.01	60.44 \pm 3.76	58.80 \pm 1.31	57.55 \pm 2.64	56.40 \pm 5.09
SimCLR	Log-mel	59.26 \pm 4.26	67.58 \pm 2.69	64.31 \pm 4.00	60.55 \pm 4.57	65.72 \pm 0.53	63.75 \pm 0.86	
	SIGNL	Wav2Vec2	10.16 \pm 2.16	10.26 \pm 0.97	9.87 \pm 1.23	9.23 \pm 1.73	8.37 \pm 2.15	7.69 \pm 1.04

TABLE V: Number of labels used in the training and development sets for ASVspoof 2021 DF, ASVspoof 5, and CFAD at different label percentages.

% Label	ASVspoof 2021 DF		ASVspoof 5		CFAD	
	Train	Dev	Train	Dev	Train	Dev
5%	1,269	1,242	9,117	2,838	1,920	720
10%	2,538	2,484	18,235	5,677	3,840	1,440
30%	7,614	7,453	54,707	17,031	11,520	4,320
50%	12,690	12,422	91,178	28,386	19,200	7,200
80%	20,304	19,875	145,885	45,418	30,720	11,520
Full	25,380	24,844	182,357	56,773	38,400	14,400

simulates real-world deployment in data mining applications. The results, shown in Table IV, reveal that SIGNL consistently demonstrates strong generalization, achieving the lowest EER in most configurations. For example, it achieved an EER of 10.89% when trained on ASVspoof 2021 DF with full labels and 7.69% when trained on CFAD—despite, despite the different languages used for training and testing in this cross-

domain setting. For this different language scenario, robust performance is also observed in other supervised methods using Wav2Vec2 as a front-end, likely due to Wav2Vec2’s pre-training on multilingual data, which enhances its ability to produce learnable visual representations of audio.

In limited label scenarios, SIGNL performed well, achieving EERs of 14.85% with 5% labels on ASVspoof 2021 DF and 10.16% with 5% labels on CFAD. However, in some configurations, other methods outperformed SIGNL. For instance, AASIST with different front-ends surpassed SIGNL when trained on ASVspoof 2021 DF with 30% and full label configurations. Similarly, AASIST and LCNN with Wav2Vec2 as the front-end outperformed SIGNL when trained on CFAD with 30% label data.

The results indicate that *cross-domain evaluation poses greater challenges than in-domain evaluation*, as evidenced by generally poorer performance on ASVspoof 5 across all baselines. This likely stems from the models not encountering

TABLE VI: EER (%) comparison for SIGNL across different combinations of graph augmentations in the full-label scenario. All values represent mean \pm standard deviation. Lower values: better performance (\downarrow). **Bold**: best result.

Methods	ED	GN	FM	ASVspoof 2021 DF	ASVspoof 5	CFAD
SIGNL-1	-	-	-	8.57 \pm 1.65	2.72 \pm 0.94	8.63 \pm 0.30
SIGNL-2	-	-	\checkmark	9.19 \pm 1.45	3.25 \pm 1.46	8.80 \pm 0.41
SIGNL-3	-	\checkmark	-	7.93 \pm 0.54	2.59 \pm 0.44	8.83 \pm 0.39
SIGNL-4	-	\checkmark	\checkmark	8.80 \pm 1.24	2.53 \pm 1.07	8.64 \pm 0.11
SIGNL-5	\checkmark	-	-	8.02 \pm 0.73	2.89 \pm 1.13	8.58 \pm 0.21
SIGNL-6	\checkmark	-	\checkmark	9.00 \pm 2.52	2.42 \pm 0.96	8.89 \pm 0.47
SIGNL-7	\checkmark	\checkmark	-	9.40 \pm 2.98	2.86 \pm 0.75	8.57 \pm 0.25
SIGNL-8	\checkmark	\checkmark	\checkmark	7.21 \pm 0.61	2.33 \pm 0.66	8.44 \pm 0.12

the relevant characteristics of novel or unseen audio attack types during pre- and downstream training, highlighting the difficulty of generalizing to *out-of-distribution (OOD) attacks*. Further discussion of this issue is provided in subsection V-H.

E. (RQ2) Analysis on Graph Augmentations

To address RQ2, we evaluated all possible combinations of three graph augmentations: Edge Dropping (ED), Gaussian Noise (GN), and Feature Masking (FM) on the ASVspoof 2021 DF and ASVspoof 5 datasets. The parameters were configured as follows: an edge-dropping probability of 0.5, a Gaussian noise standard deviation of 0.1, and a feature masking probability of 0.5. We tested eight different experimental configurations, as outlined in Table VI. The results indicate that the SIGNL-8 variant, which applies all three augmentation techniques (ED, GN, and FM), achieved the best performance. Specifically, SIGNL-8 obtained the lowest EER scores, with 7.21% on the ASVspoof 2021 DF, 2.33% on the ASVspoof 5, and 8.44% on the CFAD datasets. These findings highlight the effectiveness of combining multiple augmentation techniques, as it enhances the quality of SIGNL’s representation learning during the pre-training process and improves its ability to detect audio deepfakes.

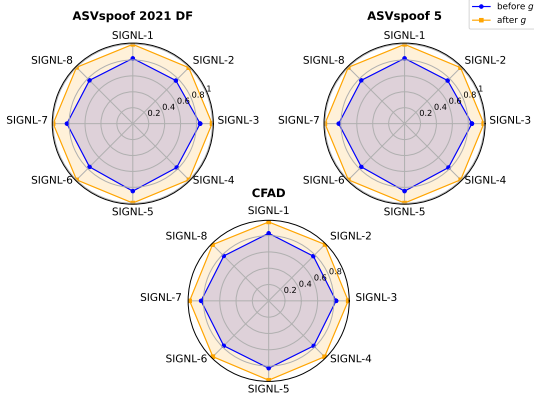


Fig. 3: Similarity of the pair embeddings before and after the projection head g .

Analysis on Feature Collapse. A well-known challenge in contrastive learning is feature collapse, which occurs when the encoder generates identical features for all inputs, leading

to a failure in learning meaningful representations [29]. This typically happens when the learning process relies solely on positive pairs without negative samples to introduce diversity. However, recent studies show that graph non-contrastive learning can avoid feature collapse in graph-level tasks, even without additional architectural modifications [29].

To validate this, we analyzed our model variants under different augmentation configurations by measuring the similarity of feature embeddings before and after passing through the projection head g . As shown in Figure 3, SIGNL’s various augmentation settings effectively prevent feature collapse. Although the projection head g produces highly similar features (indicating a collapsed solution) with nearly perfect similarity scores, the similarity of the feature embeddings *before projection* remains low, around 0.8 or less. Furthermore, the use of FM augmentation further reduces the similarity of feature embeddings, achieving scores closer to 0.7, as observed in variants SIGNL-2, SIGNL-4, SIGNL-6, and SIGNL-8. These overall pair similarity visualizations suggest that the encoders are effectively learning diverse and meaningful representations and are not suffering from collapse.

It is also important to note that the projection head is removed after pre-training, which is in line with common practices, ensuring that the learned representations are not affected by the collapsed outputs of the projection head during the downstream tasks.

F. (RQ3) Ablation Studies

To address RQ3, we conducted ablation experiments by selectively removing specific components from our framework to assess their contribution. We evaluated the following five ablation settings:

- **Without Vision GC Encoders (SIGNL w/o GNN):** In this setting, we replace the vision graph convolution (GC) encoders with a CNNs-based model, eliminating graph techniques.
- **Without Temporal Graph (SIGNL w/o G_t):** Here, we exclude the temporal graph utilization and use only the spatial graph for model training.
- **Without Spatial Graph (SIGNL w/o G_s):** In this configuration, we manage to remove the spatial graph and rely solely on the temporal graph.
- **Without fine-tuning (SIGNL w/o FT):** We adopt a fixed approach where the pre-trained encoder parameters remain unchanged during downstream training.
- **Without Pre-training (SIGNL w/o Pre):** In this setting, we skip the pre-training phase and directly perform downstream training without leveraging graph-based augmentations used in pre-training.

The results of these ablation studies are shown in Table VII. When the vision GC encoders are replaced with a CNN-based model, the EER increases to 13.28% for ASVspoof 2021 DF, 9.42% for ASVspoof 5, and 10.59% for CFAD, highlighting the importance of vision GC encoders. These results demonstrate that vision GC encoders capture complex interactions between patches in the visual representation of

TABLE VII: EER (%) comparison for SIGNL under various ablation settings in the full-label scenario. All values represent mean \pm standard deviation. Lower values: better performance (\downarrow). **Bold**: best result.

Methods	ASVspooF 2021 DF	ASVspooF 5	CFAD
SIGNL w/o GNN	13.28 \pm 1.13	9.42 \pm 2.93	10.59 \pm 0.97
SIGNL w/o G^T	8.93 \pm 0.74	4.57 \pm 1.48	10.75 \pm 0.41
SIGNL w/o G^S	10.81 \pm 0.91	10.12 \pm 3.14	11.22 \pm 0.88
SIGNL w/o FT	9.23 \pm 0.82	5.36 \pm 1.67	15.18 \pm 1.33
SIGNL w/o Pre	7.91 \pm 0.73	2.61 \pm 0.87	8.62 \pm 1.14
SIGNL	7.21 \pm 0.61	2.33 \pm 0.66	8.44 \pm 0.12

audio, unlike CNNs, which primarily focus on local patterns without modeling intricate relationships.

Furthermore, utilizing both temporal and spatial graph structures enhances performance instead of relying on a single type of graph. Excluding the temporal graph G^T raises the EER to 8.93% for ASVspooF 2021 DF, 4.57% for ASVspooF 5, and 10.75% for CFAD, while excluding the spatial graph G^S results in an EER of 10.81% for ASVspooF 2021 DF, 10.12% for ASVspooF 5, and 11.22% for CFAD. This demonstrates that modeling interdependencies on both temporal and spatial graphs provides a more comprehensive data representation, improving audio deepfake detection.

The EER increases to 9.23% for ASVspooF 2021 DF, 5.36% for ASVspooF 5, and 15.18% when the fine-tuning approach is not used, highlighting its essential role in adjusting the pre-trained encoders to accommodate audio deepfake detection tasks. Similarly, skipping the label-free pre-training process raises the EER to 7.91% for ASVspooF 2021 DF, 2.61% for ASVspooF 5, and 8.62% for CFAD, showing that pre-training helps encoders learn latent representations from various graph characteristics before downstream training, which is done without requiring any labels.

In summary, the complete SIGNL framework outperforms its ablated versions, confirming the necessity of each component: the vision GC encoders, spatio-temporal graph structures, fine-tuning, and pre-training.

G. (RQ4) Parameter Sensitivity

Sensitivity Analysis of Hyperparameters. When converting the visual representation of audio into graph data, the number of patches, N , serves as a key hyperparameter that determines the number of nodes in both spatial and temporal graphs. To maintain consistency between spatial and temporal views, we use the same number of patches for both. We experimented with different patch sizes N based on common divisors of the dimensions of the visual feature produced by Wav2Vec2 which is (1024, 224). The observed common divisors of 1024 and 224 are 4, 8, 16, and 32. In addition to patch size, we analyzed the impact of the number of neighbors K , another critical hyperparameter that controls the graph’s connectivity by defining the number of relationships each node maintains. This parameter affects the graph’s density, influencing its structure and characteristics. We tested K values ranging from 1 to 7. As shown in Figure 4, the best results across all datasets were achieved with $N = 32$. Specifically, for the ASVspooF

2021 DF dataset, the lowest EER (7.21%) was obtained with $K = 3$. Similarly, for ASVspooF 5, the best EER (2.33%) was achieved with $K = 3$, and for CFAD, the lowest EER (8.44%) occurred with $K = 4$.

Impact of Different Visual Representations. Converting raw audio into fixed-length representations, such as matrices, is crucial for information retrieval of audio data. This process captures the time-frequency characteristics of audio signals, enabling data mining techniques to analyze and extract meaningful patterns more effectively. These matrices can be visualized as heatmaps or other types of plots. We evaluated several visual representations, including Linear Frequency Cepstral Coefficients (LFCC), Mel-Frequency Cepstral Coefficients (MFCC), and Log-mel spectrogram. Additionally, we tested visual inputs derived from pre-trained SSL models, namely Whisper [35] and Wav2Vec2 [34]. Whisper’s ”tiny” variant and Wav2Vec2’s ”wav2vec2-xls-r-300m” variant were used to generate learnable visual representations of audio data. As shown in Figure 5, the Wav2Vec2 as visual representation delivered the best performance, yielding the lowest EER values across the datasets.

H. Discussion and Future Directions

While SIGNL successfully addresses the challenges of limited labeled data through graph data augmentation and non-contrastive learning, some limitations remain. A key challenge is the *generalization to out-of-distribution (OOD) attacks*—a common issue across audio deepfake detection model—as shown in the cross-domain evaluation when trained using ASVspooF 5. It is difficult to ensure robust performance when encountering novel or previously unseen attack types. Thus, ensuring data quality and variability during representation learning is crucial for improving generalization across diverse attack scenarios.

Our *analysis of graph augmentations (RQ2)* demonstrates that techniques such as edge dropping, Gaussian noise, and feature masking increase the diversity of multi-view graphs, allowing the model to capture different data characteristics during pre-training. Importantly, the results from our *ablation studies (RQ3)* show that downstream fine-tuning realigns the model with the primary task of audio deepfake detection, ensuring that these augmentations do not adversely affect the model’s performance. Although SIGNL reduces dependence on labeled data, *pre-training still requires access to a sufficient amount of unlabeled data* to generate high-quality representations and robust encoders. In scenarios where both labeled and unlabeled data are limited, the model’s performance may be impacted, especially when detecting unseen attack types. However, this challenge is not unique to SIGNL—most state-of-the-art models in audio deepfake detection face similar data-related constraints.

Addressing these limitations presents opportunities for *future research*. Techniques such as *domain adaptation*, *few-shot learning*, and *continual learning* could further enhance the model’s ability to generalize to OOD attacks [49], [50]. Additionally, exploring more efficient pre-training strategies or

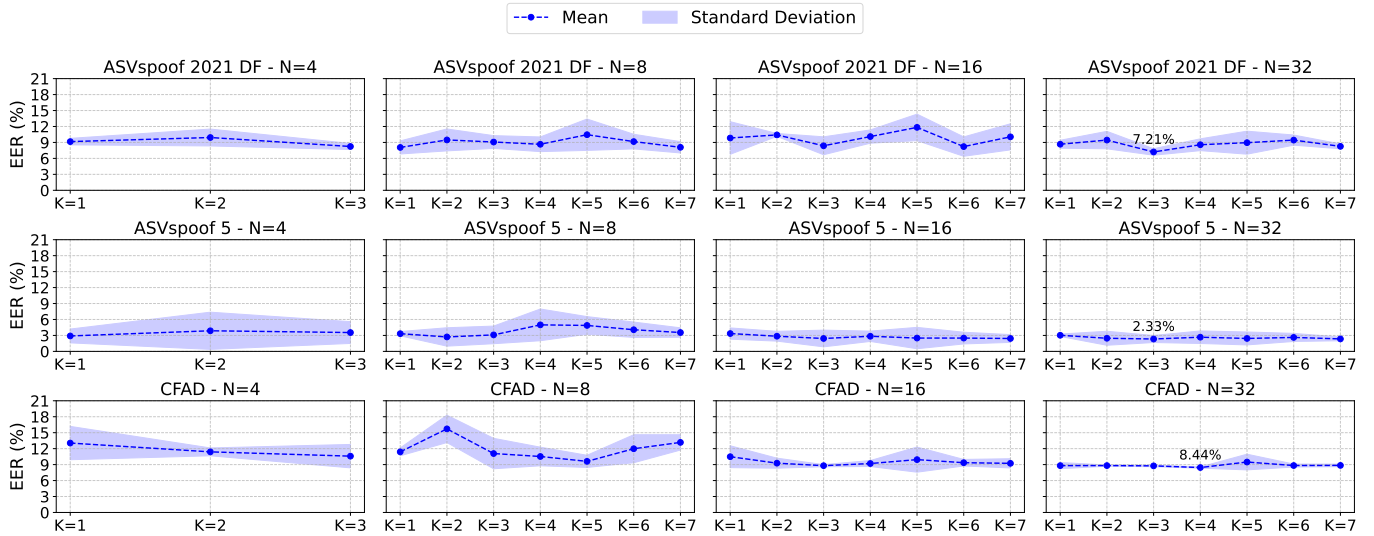


Fig. 4: EER (%) comparison for SIGNAL across different combinations of the number of patches (N) and the number of node’s neighbors (K) in the full-label scenario. The line plots represent the mean EER values, while the shaded areas indicate the standard deviation. Lower values: better performance (\downarrow).

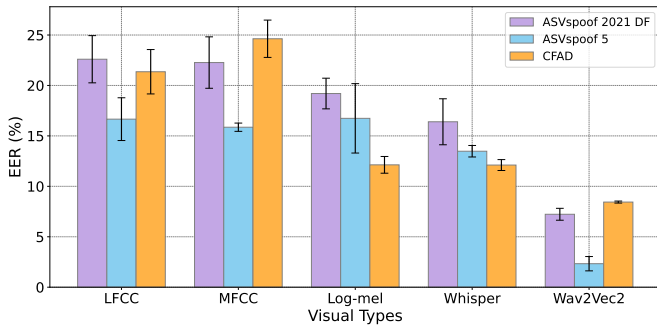


Fig. 5: EER (%) comparison for SIGNAL across different visual representations of audio in the full-label scenario. The bar charts represent the mean, while the error bars indicate the standard deviation. Lower values: better performance (\downarrow).

advanced self-supervised approaches may improve adaptability and scalability in data-constrained environments.

VI. CONCLUSION

In this work, we introduced SIGNAL, a graph-based, non-contrastive learning technique for audio deepfake detection that addresses the challenges of limited labeled data. Our approach performs data management to construct temporal-spatial graph structures from a visual representation of audio data, applying graph-based augmentations during pre-training to enhance data variation. We pre-train our vision graph convolutional (GC) encoders using the non-contrastive learning strategy, enabling a label-free training process. In the downstream task, we fine-tune these pre-trained encoders with limited labeled data for effective audio deepfake detection. Extensive experiments show that SIGNAL outperforms the baselines in the ASVspoof 2021 DF, ASVspoof 5, and CFAD datasets,

and also for In-the-Wild dataset for cross-domain evaluation, achieving high performance even when only 5% of labeled data is used.

REFERENCES

- [1] X. Tan, J. Chen, H. Liu, J. Cong, C. Zhang, Y. Liu, X. Wang, Y. Leng, Y. Yi, L. He *et al.*, “Naturalspeech: End-to-end text-to-speech synthesis with human-level quality,” *IEEE Transactions on Pattern Analysis and Machine Intelligence*, 2024.
- [2] K. Wang, J. Zhang, Y. Ren, M. Yao, D. Shang, B. Xu, and G. Li, “Spikevoice: High-quality text-to-speech via efficient spiking neural network,” in *Proceedings of the 62nd Annual Meeting of the Association for Computational Linguistics (Volume 1: Long Papers)*, 2024, pp. 7927–7940.
- [3] H.-Y. Choi, S.-H. Lee, and S.-W. Lee, “Dddm-vc: Decoupled denoising diffusion models with disentangled representation and prior mixup for verified robust voice conversion,” in *AAAI*, 2024.
- [4] V. Popov, I. Vovk, V. Gogoryan, T. Sadekova, M. S. Kudinov, and J. Wei, “Diffusion-based voice conversion with fast maximum likelihood sampling scheme,” in *ICLR*, 2021.
- [5] B. Sisman, J. Yamagishi, S. King, and H. Li, “An overview of voice conversion and its challenges: From statistical modeling to deep learning,” *IEEE/ACM Transactions on Audio, Speech, and Language Processing*, vol. 29, pp. 132–157, 2020.
- [6] J. Yi, C. Wang, J. Tao, X. Zhang, C. Y. Zhang, and Y. Zhao, “Audio deepfake detection: A survey,” *arXiv preprint arXiv:2308.14970*, 2023.
- [7] R. Ranjan, M. Vatsa, and R. Singh, “Uncovering the deceptions: an analysis on audio spoofing detection and future prospects,” in *IJCAI*, 2023.
- [8] H. Tak, J. Patino, M. Todisco, A. Nautsch, N. Evans, and A. Larcher, “End-to-end anti-spoofing with rawnet2,” in *ICASSP*, 2021.
- [9] Z. Wu, R. K. Das, J. Yang, and H. Li, “Light convolutional neural network with feature genuinization for detection of synthetic speech attacks,” in *INTERSPEECH*, 2020.
- [10] T. Chen, E. Khoury, K. Phatak, and G. Sivaraman, “Pindrop labs’ submission to the asvspoof 2021 challenge,” *Proc. 2021 Edition of the Automatic Speaker Verification and Spoofing Countermeasures Challenge*, pp. 89–93, 2021.
- [11] K. He, X. Zhang, S. Ren, and J. Sun, “Deep residual learning for image recognition,” in *CVPR*, 2016.
- [12] X. Liu, M. Liu, L. Wang, K. A. Lee, H. Zhang, and J. Dang, “Leveraging positional-related local-global dependency for synthetic speech detection,” in *ICASSP*, 2023.

- [13] F. Chen, S. Deng, T. Zheng, Y. He, and J. Han, "Graph-based spectro-temporal dependency modeling for anti-spoofing," in *ICASSP*, 2023.
- [14] J.-w. Jung, H.-S. Heo, H. Tak, H.-j. Shim, J. S. Chung, B.-J. Lee, H.-J. Yu, and N. Evans, "Aasist: Audio anti-spoofing using integrated spectro-temporal graph attention networks," in *ICASSP*, 2022.
- [15] K. Han, Y. Wang, J. Guo, Y. Tang, and E. Wu, "Vision gnn: An image is worth graph of nodes," *NeurIPS*, 2022.
- [16] H. Tak, J.-W. Jung, J. Patino, M. Kamble, M. Todisco, and N. Evans, "End-to-end spectro-temporal graph attention networks for speaker verification anti-spoofing and speech deepfake detection," in *ASVspoof Workshop*, 2021.
- [17] H. Tak, J.-w. Jung, J. Patino, M. Todisco, and N. Evans, "Graph attention networks for anti-spoofing," in *INTERSPEECH*, 2021.
- [18] Q. Zhang, S. Wen, and T. Hu, "Audio deepfake detection with self-supervised xls-r and sls classifier," in *Proceedings of the 32nd ACM International Conference on Multimedia*, 2024, pp. 6765–6773.
- [19] H. Tak, M. Todisco, X. Wang, J.-w. Jung, J. Yamagishi, and N. Evans, "Automatic speaker verification spoofing and deepfake detection using wav2vec 2.0 and data augmentation," in *Proc. The Speaker and Language Recognition Workshop (Odyssey)*, 2022.
- [20] Z. Jiang, Y. Xu, H. Xu, Z. Wang, and C. Qiao, "Clients help clients: Alternating collaboration for semi-supervised federated learning," in *ICDE*, 2024.
- [21] Y. Liu, M. Jin, S. Pan, C. Zhou, Y. Zheng, F. Xia, and S. Y. Philip, "Graph self-supervised learning: A survey," *IEEE transactions on knowledge and data engineering*, vol. 35, no. 6, pp. 5879–5900, 2022.
- [22] L. Ericsson, H. Gouk, C. C. Loy, and T. M. Hospedales, "Self-supervised representation learning: Introduction, advances, and challenges," *IEEE Signal Processing Magazine*, vol. 39, no. 3, pp. 42–62, 2022.
- [23] J. Yamagishi, X. Wang, M. Todisco, M. Sahidullah, J. Patino, A. Nautsch, X. Liu, K. A. Lee, T. Kinnunen, N. Evans *et al.*, "Asvspoof 2021: accelerating progress in spoofed and deepfake speech detection," in *ASVspoof Workshop*, 2021.
- [24] H.-s. Shin, J. Heo, J.-h. Kim, C.-y. Lim, W. Kim, and H.-J. Yu, "Hm-conformer: A conformer-based audio deepfake detection system with hierarchical pooling and multi-level classification token aggregation methods," in *ICASSP*, 2024.
- [25] K. Ding, Z. Xu, H. Tong, and H. Liu, "Data augmentation for deep graph learning: A survey," *ACM SIGKDD Explorations Newsletter*, vol. 24, no. 2, pp. 61–77, 2022.
- [26] J.-B. Grill, F. Strub, F. Altché, C. Tallec, P. Richemond, E. Buchatskaya, C. Doersch, B. Avila Pires, Z. Guo, M. Gheshlaghi Azar *et al.*, "Bootstrap your own latent—a new approach to self-supervised learning," *NeurIPS*, 2020.
- [27] X. Chen and K. He, "Exploring simple siamese representation learning," in *CVPR*, 2021.
- [28] C. Liu, K. Li, M. Stopa, J. Amano, and Y. Fu, "Discovering informative and robust positives for video domain adaptation," in *ICLR*, 2022.
- [29] X. Guo, Y. Wang, Z. Wei, and Y. Wang, "Architecture matters: Uncovering implicit mechanisms in graph contrastive learning," *NeurIPS*, 2024.
- [30] W. Ju, Y. Wang, Y. Qin, Z. Mao, Z. Xiao, J. Luo, J. Yang, Y. Gu, D. Wang, Q. Long *et al.*, "Towards graph contrastive learning: A survey and beyond," *arXiv preprint arXiv:2405.11868*, 2024.
- [31] R. Li, S. Di, L. Chen, and X. Zhou, "Gradgcl: Gradient graph contrastive learning," in *ICDE*, 2024.
- [32] P. Veličković, G. Cucurull, A. Casanova, A. Romero, P. Liò, and Y. Bengio, "Graph attention networks," in *ICLR*, 2018.
- [33] M. Welling and T. N. Kipf, "Semi-supervised classification with graph convolutional networks," in *ICLR*, 2017.
- [34] A. Baevski, Y. Zhou, A. Mohamed, and M. Auli, "wav2vec 2.0: A framework for self-supervised learning of speech representations," *NeurIPS*, 2020.
- [35] A. Radford, J. W. Kim, T. Xu, G. Brockman, C. McLeavey, and I. Sutskever, "Robust speech recognition via large-scale weak supervision," in *ICLR*, 2023.
- [36] T. Chen, S. Kornblith, M. Norouzi, and G. Hinton, "A simple framework for contrastive learning of visual representations," in *ICML*, 2020.
- [37] K. He, H. Fan, Y. Wu, S. Xie, and R. Girshick, "Momentum contrast for unsupervised visual representation learning," in *CVPR*, 2020.
- [38] H. Zhang, Y. Zou, and H. Wang, "Contrastive self-supervised learning for text-independent speaker verification," in *ICASSP*, 2021.
- [39] W. Xia, C. Zhang, C. Weng, M. Yu, and D. Yu, "Self-supervised text-independent speaker verification using prototypical momentum contrastive learning," in *ICASSP*, 2021.
- [40] A. Saeed, D. Grangier, and N. Zeghidour, "Contrastive learning of general-purpose audio representations," in *ICASSP*, 2021.
- [41] S. Wang, S. Tripathy, and A. Mesaros, "Self-supervised learning of audio representations using angular contrastive loss," in *ICASSP*, 2023.
- [42] D. Niizumi, D. Takeuchi, Y. Ohishi, N. Harada, and K. Kashino, "Byol for audio: Exploring pre-trained general-purpose audio representations," *IEEE/ACM Transactions on Audio, Speech, and Language Processing*, vol. 31, pp. 137–151, 2022.
- [43] A. v. d. Oord, Y. Li, and O. Vinyals, "Representation learning with contrastive predictive coding," *arXiv preprint arXiv:1807.03748*, 2018.
- [44] X. Wang, H. Delgado, H. Tak, J.-w. Jung, H.-j. Shim, M. Todisco, I. Kukanov, X. Liu, M. Sahidullah, T. Kinnunen *et al.*, "Asvspoof 5: Crowdsourced speech data, deepfakes, and adversarial attacks at scale," *arXiv preprint arXiv:2408.08739*, 2024.
- [45] H. Ma, J. Yi, C. Wang, X. Yan, J. Tao, T. Wang, S. Wang, and R. Fu, "Cfad: A chinese dataset for fake audio detection," *Speech Communication*, vol. 164, p. 103122, 2024.
- [46] N. M. Müller, P. Czempin, F. Dieckmann, A. Froggyar, and K. Böttinger, "Does audio deepfake detection generalize?" in *INTERSPEECH*, 2022.
- [47] M. Todisco, X. Wang, V. Vestman, M. Sahidullah, H. Delgado, A. Nautsch, J. Yamagishi, N. Evans, T. Kinnunen, and K. A. Lee, "Asvspoof 2019: Future horizons in spoofed and fake audio detection," in *INTERSPEECH*, 2019.
- [48] P. Kawa, M. Plata, M. Czuba, P. Szymański, and P. Syga, "Improved deepfake detection using whisper features," 2023.
- [49] X. Li and L. Chen, "Graph anomaly detection with domain-agnostic pre-training and few-shot adaptation," in *ICDE*. IEEE, 2024.
- [50] F. G. Febrinanto, F. Xia, K. Moore, C. Thapa, and C. Aggarwal, "Graph lifelong learning: A survey," *IEEE Computational Intelligence Magazine*, vol. 18, no. 1, pp. 32–51, 2023.